Novel procedure for studying laser-surface material interactions during scanning laser ablation cleaning processes on Cu-based alloys

Novel procedure for studying laser-surface material interactions during scanning laser ablation cleaning processes on Cu-based alloys

Elisabetta Di Francia[a**], Ruth Lahoz[b*], Delphine Neff[c], Victor Rico[d], Nicolas Nuns[e], Emma Angelini[a], Sabrina Grassini[a]

[a] Politecnico di Torino, Dipartimento di Scienza Applicata e Tecnologia, Corso Duca degli Abruzzi 24, 10129 Torino, Italy (elisabetta.difrancia@polito.it, sabrina.grassini@polito.it, emma.angelini@polito.it)

[b] Instituto de Nanociencia y Materiales de Aragón (INMA), CSIC - Universidad de Zaragoza, María de Luna 3, 50018 Zaragoza, Spain (rlahoz@unizar.es)

[c] NIMBE/LAPA-IRAMAT, CEA/CNRS/Université Paris-Saclay, UMR3685, CEA Saclay, bat 637, 91191 Gif/Yvette, France (delphine.neff@cea.fr)

[d] Instituto de Ciencia de Materiales de Sevilla (CSIC), Avenida Americo Vespucio, 49, 41092 Sevilla, Spain (victor@icmse.csic.es)

[e] Univ. Lille, CNRS, INRA, Centrale Lille, ENSCL, Univ. Artois, FR 2638 - IMEC - Michel-Eugène Chevreul, F-59000 Lille, France (nicolas.nuns@univ-lille1.fr)

Corresponding authors:

* Ruth Lahoz (rlahoz@unizar.es) ORCID: 0000-0003-4708-5577

** Elisabetta Di Francia (elisabetta.difrancia@polito.it) ORCID: 0000-0003-1874-7543

Abstract

Laser ablation is an effective method to clean Cu-based alloys. A novel procedure of characterisation was developed involving ^{18}O isotopes evaluated by ToF-SIMS spectroscopy to assess the driving mechanisms of laser-surface interactions. The presence of re-oxidised compounds was detected, discerning between the oxygen from the corrosion layer and the one introduced by the interaction with the laser (that was generated in a controlled atmosphere of ^{18}O diluted in N_2). A set of samples treated with different laser conditions were characterised by FESEM and μRaman. The results have shown that re-oxidation phenomenom can occur and its selectivity depends on the laser conditions.

Keywords: laser ablation; copper alloys; corrosion; surface interaction mechanisms; ToF-SIMS

Funding: This research did not receive any specific grant from funding agencies in the

public, commercial, or not-for-profit sectors.

1. Introduction

Laser technology is widely used in materials processing for industrial applications: e.g., cutting and marking, drilling, welding, material ablation [1,2]. In particular, surface cleaning by laser ablation has applications in several fields: e.g., the stripping of paint for making barrier between the environment and the surface [2], the cleaning of oil lubricants, rust or paint from surfaces in steel manufacturing [3,4], the elimination of carbonaceous deposits on engine parts [5]. And of course, the removal of continuous layers or particles from metallic surfaces (stainless steel, silicon wafer, aluminium alloy) [6,7].

However, limited information is available within the literature on laser-surface material interactions during the elimination of corrosion layers on metals, in particular the laser-induced removal of corrosion products on Cu-based alloys. For example, Zhang and collaborators reported that, on aluminium alloy, laser ablation is able to remove an original and less protective passivation layer creating a more protective one [7].

Laser-material interaction mechanisms constitute a very important field of study in laser materials processing. Those interactions have different classification options within the science community. One of the most related to the laser parameters is the one that links the main interactions to the duration of the irradiation (in continuous lasers) or the laser pulse duration (in pulsed lasers) [8]. This last one classifies the laser-interaction mechanisms mainly into thermal, photo-thermal, photo-physical and athermal, as the laser pulse duration decreases. Most industrial applications mentioned before, included cleaning, are performed with medium-long pulse durations (between 4 to 200 ns). This means that thermal related mechanism govern the ablation process.

So it is accepted that the laser ablation mechanism during cleaning procedures is mainly driven by the thermal mechanism induced by nanosecond infrared irradiation.

Moreover, for nanosecond pulsed lasers, the lattice heat diffusion is the dominant transport mechanism [6]. Schou and co-workers [9] proposed a model in four stages for the ablation process using laser pulses in the nanosecond regime:

- A (*laser-solid interactions*), the laser beam strikes the solid and it is absorbed by the electrons/atoms with a consequent strong heating of the irradiated volume;
- B (*laser-plasma interactions*), at this stage the material is ejected from the heated volume and continues to absorb laser energy forming a thin layer of ionised vapour;

- C (*plume formation*), at the end of the laser pulse, the expansion of the plasma plume occurs in different way in vacuum or background gas;
- D, in presence of background gas, interactions of the plume atoms with the atoms and molecules of the gas determine the plume expansion.

In addition to this, if the average power per area (*irradiance*) exceeds some threshold irradiance values, multiphoton, ionisations or thermal processes result in a dense cloud of electrons and ionised species within the laser focus. If the collision number between charge carriers is larger than the number of collision between the crystallographic lattice and the charge carriers, the charge carriers present a collective behaviour and they form the plasma. The extension and the shape of the plasma plume depend on the laser fluence [6]. In those conditions, the energy of the plasma plume is so high that it allows the ionisation and so the removal of surface material as liquid, vapour or solid clusters. Hence, the physical parameters in the plume (e.g. the mass distribution, ion and atom velocity) are important to know in the laser ablation study since they can regulate the affected depth in the bulk. However, the interactions between the species in the plume and the interactions between the species and the laser beam are very complex to be modelled and explained, depending on the interaction atmosphere [9].

Furthermore, the complexity of the materials irradiated with laser has made very difficult to assign just one interaction to the laser process. This is even more complex when considering the case of multi-component systems, as the corrosion products which can grow on Cu-based alloys under a long period of time in various media, as soil, marine or freshwater, or atmosphere: they are constituted by an inner dense copper oxide layer and, generally, an outer porous layer constituted by an heterogeneous mixture of chloride/carbonate/sulphide/sulphate compounds [10–13]. These different corrosion products normally differ in their optical and thermal properties.

If, during the laser process, melting occurs, a solid-state diffusion of species may take place especially in multi-component systems. This can result in changes in the chemical composition. In this case, not only the corrosion products may be affected but also the metallic substrate, if the heat diffusion reaches the first layers of the bulk material [14]. In recent decades, laser cleaning has also been used to eliminate selectively corrosion layers in the field of Conservation of Cultural Heritage. But these studies are in general more focused on the success of the ablation process; the ablation mechanisms

themselves have been considered only in very few cases [15–18].
Previous systematic characterisation carried out by these authors on laser-cleaning tests showed no changes in the composition of the corrosion layers before and after the laser-cleaning treatments [19]. Typical results, observed by many authors in the laser community, show that the materials found on the metal surface after cleaning are either inner corrosion layers revealed after the ablation of the outer ones [20–22], or new materials generated because of a re-oxidation of the ablated surface layers [5,7,23–25], or the combination of both. Ejected materials, that interacted within the plasma plume and the atmosphere during the ablation process, and that are later re-deposited on the surface may also be found [26]. This latter seems to be less probable, on the area treated by laser, by the fact that several studies reported that no significant chemical changes take place within the reductive atmosphere of the plasma plume, especially under infrared irradiation [8,27], and that the ablated material is commonly ejected outwards the irradiated area. Despite this, interactions among the ablated species and among the ablated species and the laser pulses cannot be denied either. If this happens, it will probably be related to the high temperature values reached and the thermal conductivity. Nevertheless, when the plasma plume disappears, the reactive ablated species are expected to turn to the most stable state. The novel experimental procedure here designed and proposed aims to clarify if the second described phenomenon (re-oxidation) is occurring, since there are no chemical changes observed.
In this work, a NIR Q-switched Yb:YAG fibre laser operating in the nanosecond pulsed regime has been tested on a set of artificially-corroded Cu-based reference samples. To assess the ablation mechanisms and the presence of possible laser-surface material interactions of the surface layer with the oxygen present in the air during the laser interaction, laser treatments were carried out in synthetic air marked by ^{18}O, a less abundant oxygen isotope of the atmosphere (0.205(14) at.% [28]). Subsequently, advanced ToF-SIMS (Time-of-Flight Secondary Ion Mass Spectrometry) analysis was performed to detect a possible enrichment in ^{18}O in the laser-treated layers. Laser parameters were selected to force the possible re-oxidation phenomena among the reactive radicals, present on the ablated surface, and the oxygen present in the synthetic air during laser irradiation. The characterisation conducted on the irradiated areas is discussed and a model of the laser-surface and material-atmosphere interaction mechanisms during the ablation process is proposed. Verifying the presence of re-oxidised compounds, due to possible interactions of the surface materials with the

oxygen present in the air during the laser treatment, is of fundamental importance to assess the mechanisms of the cleaning procedure. As a matter of fact, if a re-oxidation of the ablated surface occurs, the ^{18}O isotope is incorporated in the surface layer, which therefore should be enriched by an abnormal ^{18}O percentage. From the results obtained through the used experimental set-up, an ablation model for the laser-cleaning test in synthetic air can be proposed. The re-deposition phenomenon, outside the laser-treated zones, and the incorporation of ^{18}O in this re-deposited material are not the subject of this study.

2. Materials and methods

2.1. Artificially-corroded Cu reference samples

Artificially-corroded Cu reference samples with a tailored chemical composition, microstructure, morphology, texture and colour of the corrosion products layers were produced for this study. The reference samples were chosen because they allow determining the ablation mechanism and, therefore, the efficiency of the laser-cleaning treatments by investigating the effect of the laser parameters on the different corrosion products [19].

The reference Cu specimens (99.96 wt.% Cu; 45 × 15 × 5 mm^3) were polished with 500 to 4000-grid SiC paper, rinsed in ethanol in ultrasonic bath for 5 min and well dried. Then, the reference samples were totally immersed in 0.5M NaCl solution for two months at room temperature. The solution was neither stirred nor aerated by bubbling [29].

Immediately after submitting the samples to the laser-cleaning tests, they were embedded in epoxy SpeciFix-20-Struers resin in order to avoid any air-contamination before characterisation. Cross-sections samples, with a maximum size of 20 × 15 × 5 mm^3, were obtained by cutting them in parallel to the laser scanning direction with a diamond blade and then polishing the surface until 1 μm grid cloth; ethanol was used instead of water in order to prevent any solubilisation of the corroded compounds and diamond pastes were used in conjunction with the cloths. Subsequently, the cross-sections were rinsed in isopropyl alcohol in ultrasonic bath for 10 min and well dried.

2.2. Laser-system parameters and experimental set-up

A Q-switched Yb:YAG fibre laser (Rofin laser, model PowerLine F20), operating in the near-IR region at a wavelength of 1064 nm was used. The laser pulse frequency range was from 20 kHz to 100 kHz while the pulse duration was 100 ns at 20 kHz.
The laser system was coupled via computer with EzCAD 2.1 UNI, a vector graphic editor, with a CAD-like capability that enables user to perform rapid, precise and complex surface scanning treatments in a repeatable way. In addition to this, the vector graphic editor allows not only laser parameters (e.g. output power, P, and pulse duration, t_p), but also geometrical parameters to be controlled. The Gaussian-shaped beam is focussed by a 160 mm f-Theta lens positioned after the scanning head.

Intense laser conditions, characterised by high irradiance and long pulse duration values, were chosen to force the re-oxidation phenomena among the reactive radicals present on the ablated surface and the oxygen present in the synthetic air during laser treatments. To this aim, four laser-cleaning tests were carried out with increasing values of laser irradiance, maintaining the pulse duration fixed at 200 ns. Parameter values used are displayed in Table 1.

Table 1: Test parameters chosen to force re-oxidation phenomena during laser treatments.

	Laser parameters				**Geometrical parameters**	
Test number	*Power, P (W)*	*Fluence, F (J/cm²)*	*Irradiance, I (MW/cm²)*	*Pulse Duration, t_p (ns)*	*Scanning speed, v_{scan} (mm/s)*	*Interlining, d_L (mm)*
1	0.6	4.24	21.22	200	300	0.015
2	0.9	6.37	31.83	200	300	0.015
3	1.2	8.49	42.44	200	300	0.015
4	2.1	14.85	74.27	200	300	0.015

The novel experimental procedure consisted in performing the laser-cleaning tests in a controlled atmosphere chamber filled with synthetic air (20% ^{18}O + 80% N_2), where ^{16}O is substituted completely by ^{18}O, an oxygen isotope present in small amount in natural air (0.205(14) at. %) [28]. This way, the ^{18}O trace will allow to identify if a re-oxidation of the ablated surfaces occurred.

For the laser-cleaning tests, the samples were positioned in the chamber, designed with a superior transparent window to allow the entrance of the infrared radiation. A depression of around 1 bar was done and then the chamber was filled back to recover the atmospheric pressure with synthetic air. At the end of this process, the chamber presented a controlled atmosphere constituted by ^{18}O traced synthetic air instead of natural air. A picture of the experimental set-up is shown in Figure 1.

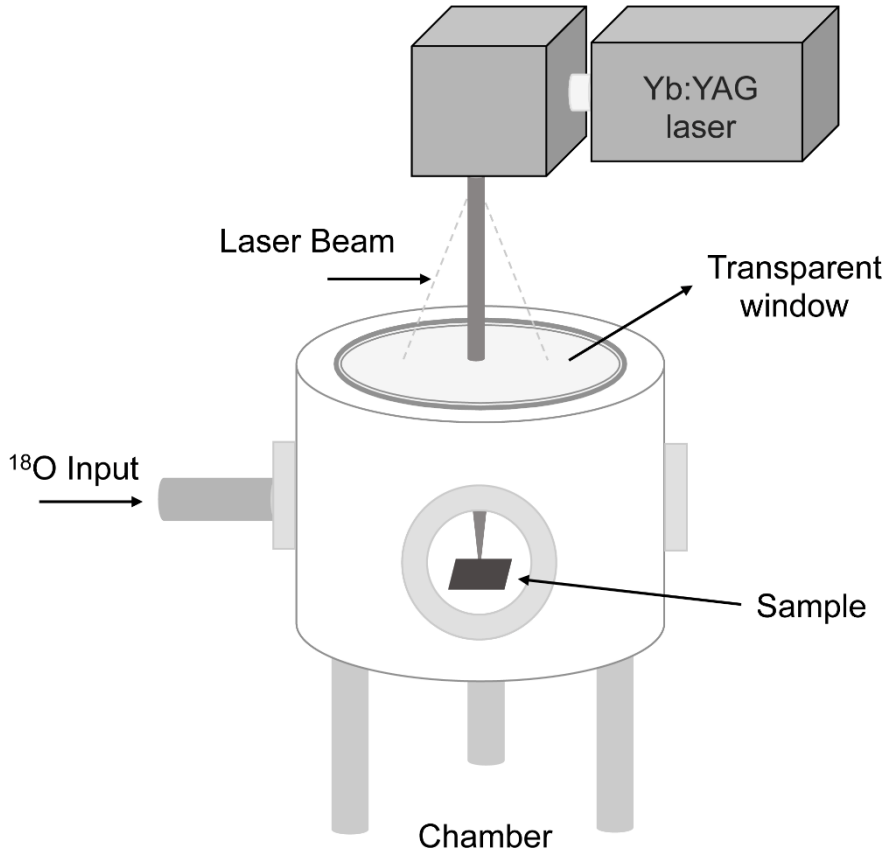

Figure 1: Laser set-up developed for the assessment of laser-surface material interaction mechanisms during ablation processes.

2.3. Characterisation techniques

Optical images were acquired by means of an Olympus BX51 optical microscope (OM) equipped with a Nikon EOS camera.

Field Emission Scanning Electron Microscopy (FESEM, Supra 40 model, Carl Zeiss, Germany) images were collected with the SMART SEM software in in-field (inLens) emission mode varying the acceleration voltage in the range of 1.5 kV to 20 kV and the working distance from 3 mm to 8.5 mm. The FESEM was coupled with an Energy

Dispersive Spectrometer (EDS INCA x-sight, Oxford instruments), equipped with INCA software, for elemental identification. EDS spectra (K and L-series characteristic of Cu, O, Cl) were acquired at 20 kV with a working distance of 8.5 mm.

μRaman analyses were performed at room temperature under a Leica x50/0.85 microscope objective and the spectra were acquired with a Renishaw Invia equipped with a doubled Nd:YAG laser (532 nm). The laser power on the sample surface was set at about 500 μW in order to avoid the thermal transformation of the analysed phases. The experimental data were compared with spectra collected in a database composed from synthetic/commercial powders obtained in laboratory and with references reported in RRUFF Project database [30] and in literature [13,31–35].

ToF-SIMS analyses were performed with a TOF.SIMS.5 instrument from IONTOF. The instrument was equipped with a Bi source for primary ions and Cs for sputtering. Before data acquisition, the surface was sputtered with Cs^+ (2 kV, 140 nA) in order to remove surface contamination. For reaching a good signal intensity, the bunch mode was firstly used for acquiring maps with a large samples areas (250 × 250 μm^2), analysed with 256 × 256 pixels and a number of scans always higher than 50.
In addition to this, in order to reach a high lateral resolution and to avoid ^{16}O detector saturation, burst mode (6 pulses, beam size ≈ 200 nm) was used; pulsed primary ions energy was 25 keV with a current of 0.1 pA. In this modality, samples areas of 75 × 75 μm^2 were analysed with 256 × 256 pixels and a number of scans always higher than 100 was used to insure a good statistic for isotopic ratio calculation. The calculation of the isotopic ratios was done by selecting *Regions Of Interest* (ROI) corresponding to the areas of the corrosion layers, as identified on the ToF-SIMS maps.
Then, the isotopic ratio percentage (O_r) was determine as follow (1) for each of the 17 acquisitions (11 different areas were analysed on Test 1 cross-sections and 2 different areas on each of Test 2 to Test 4 cross-sections):

$$O_r = \frac{^{18}O}{^{18}O + ^{16}O} \% \qquad (1)$$

where O_r is the isotopic oxygen ratio percentage; ^{18}O is the isotopic amount of ^{18}O; ^{16}O is the is the isotopic amount of ^{16}O.
For each acquisition, two source of uncertainties, strictly connected with the measurement parameters apply, were also considered:

- the ion detection uncertainty (ΔI_{cor}), calculated as (2)

$$\Delta I_{corr} = \sqrt{\frac{N\, I_{ex}}{N - I_{ex}}} \qquad (2)$$

where ΔI_{cor} is the ion detection uncertainty; N is the number of shot (measurement parameter apply); I_{ex} is the uncorrected counts;

- the uncertainties about the count statistic which is of the order of the square root of the number of detected counts of a specific element (< 0.1%, for the number of counts of a given element).

On these isotopic ratio percentage values and the correspondent errors found, the oxygen ratio estimations and the Type A, Type B and the combined uncertainties (u_C) were statistically calculated.

3. Results and discussion

3.1. Artificially-corroded layer characterisations

The artificially-corroded layers grown on the copper are schematised in Figure 2.a. The scheme shows the two differentiated layers (inner and outer) found in the cross-section that can also be observed in the FESEM cross-section image. Figure 2.a also shows a FESEM image of the surface microstructure of the outer layer. As shown, the inner layer is characterised by grain size of less than 5 µm while the outer layer is structured in bigger crystals between 5 µm to 10 µm. The characterisation by µXRD, µRaman and FESEM (described in detail in [19]), revealed that the corrosion layer is divided in an inner layer composed of cuprous and cupric oxides (Cu_2O and CuO, cuprite and tenorite), that probably grew in contact with the metal; and an outer layer composed of a polymorph of atacamite, probably clinoatacamite ($Cu_2Cl(OH)_3$)..

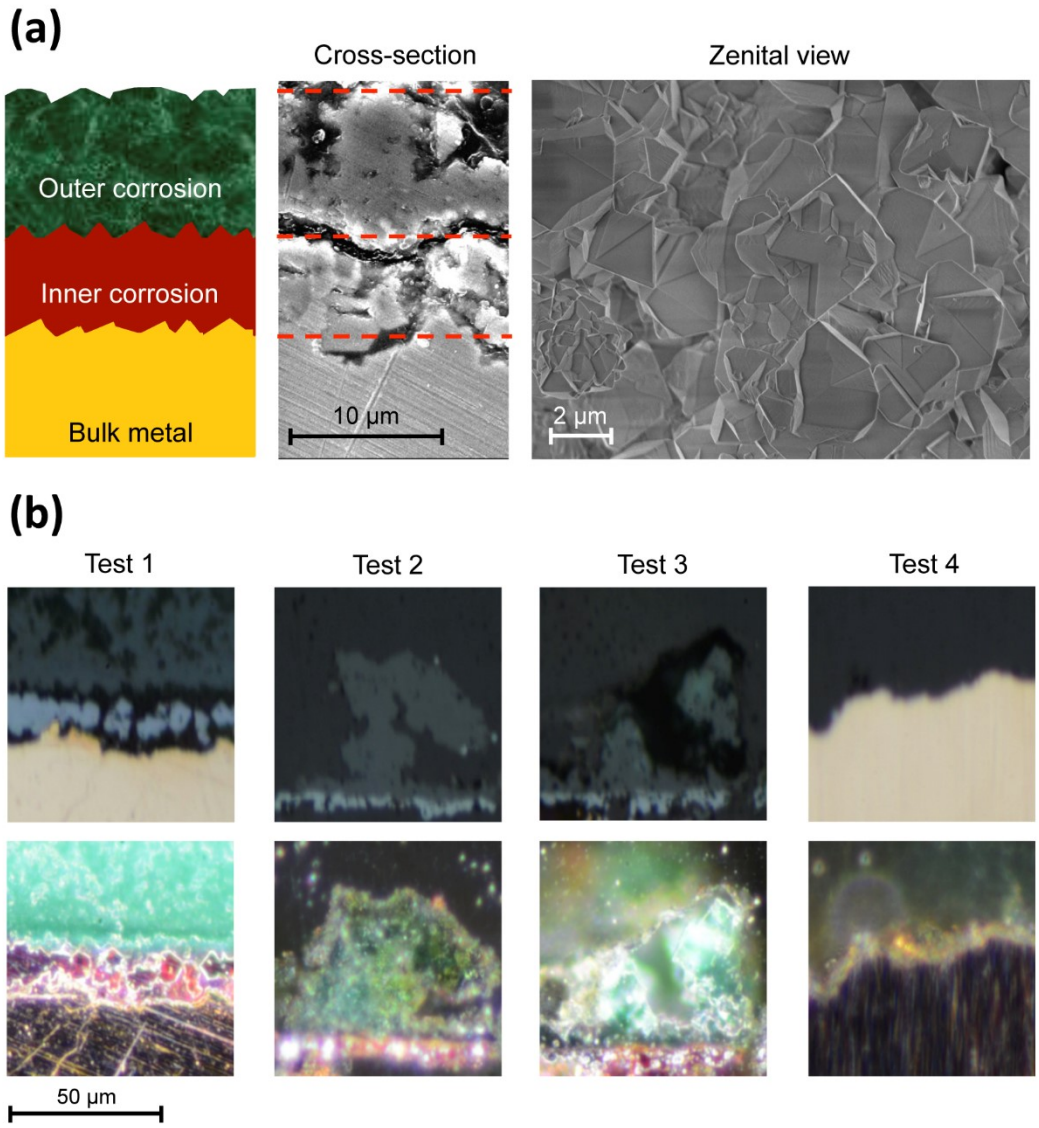

Figure 2: (a) Scheme of the cross-section of the artificially-corroded layers (inner copper oxides - Cu_2O and CuO - *layer in brown* and outer clinoatacamite - $Cu_2Cl(OH)_3$ - *layer in green*) and FESEM image corresponding to the cross-section of the corrosion products; zenital FESEM image of the outer layer surface on the right. (b) OM images of the cross-sections after the laser-cleaning tests.

As OM images (Figure 2.b) show, after the four laser tests, the inner and outer layers described for the original non-treated samples are still present after Test 1, Test 2 and Test 3. While, after Test 4, the outer layer has been completely ablated and only sporadic parts of the inner layer are present. Test 1 irradiance conditions did not remove the artificially-corroded products: an inner layer of copper oxide (light-grey) and an outer layer of hydroxychloride compounds (dark-grey) are still detectable. On the contrary, Test 4 irradiance conditions removed the whole outer layer and left only a

very thin portion of the inner layer; since the metal surface appeared rougher than the other Test samples, it suggested that it might have been also modified by the laser. Test 2 and 3 partially affected the corrosion products and both layers are still detected.

A summary of the results obtained on the characterisation conducted on the cross-sections of both non-treated and laser-treated samples is shown in Figure 3. Regarding the composition, no substantial differences were observed by comparing the data obtained on the treated samples to the non-treated one. More in details, Figure 3.a shows a comparison of the μRaman spectra acquired on outer layers (Fig. 3.d, points A) of the non-treated, Test 1 to Test 3 samples (Test 4 eliminates completely the outer layer). μRaman characterisations, performed in several points of these remaining outer layers, indicated that they were characterised by the same composition of the non-treated outer layer: an atacamite polymorph, probably clinoatacamite (peaks at 3442, 3355, 3311, 971, 930, 893, (869), 801, 514, (443-423), 366, 141 and 111cm^{-1}), as identified in [34,35]. EDS punctual analyses (Fig. 3.c, pie chart A) reinforced this hypothesis showing a typical elemental composition close to the clinoatacamite compound (22.47 wt. % O, 16.60 wt. % Cl, 59.51 wt. % Cu, 1.42 wt. % H), as reported in [36].

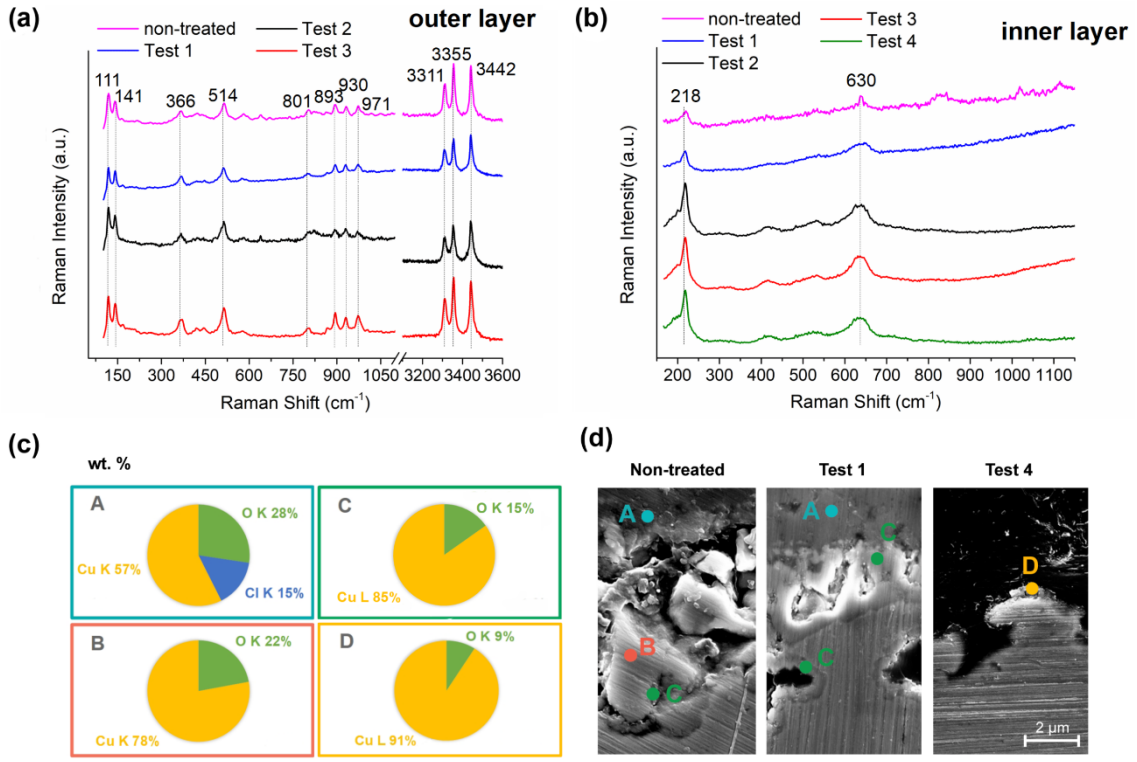

Figure 3: µRaman spectra comparing the non-treated area of the outer layer (a) and of the inner layer (b) with the four laser Tests. (c) EDS charts of selected compositional points A, B, C and D. (d) FESEM cross-section images show the position within the corrosion layers of the different compositions obtained by EDS.

Instead, the inner layer is present after Test 1 to Test 4, however the shape of the single crystals is difficult to recognise, as it is shown in Figure 3.d (points B, C and D). Figure 3.b compares the µRaman spectra acquired on the inner layer of the non-treated and the laser-treated cross-sections. While on the non-treated cross-section µRaman spectrum identified the presence of cuprite mixed with the compound of the outer layer (clinoatacamite), in several points of the Test 1 to Test 4, µRaman characterisations detected only the presence of cuprite (peaks at 630, (532), (410), 218 cm^{-1}) [13,30,31,33]. Moreover, the Figure 3 correlates the obtained spectra with the EDS average compositions (Fig.3.c) collected on the inner layers of the non-treated (Fig.3.d, points B and C), Test 1 and Test 4 (Fig.3.d, points C and D). On the non-treated inner layer, EDS analyses highlighted the presence of compositions B and C, formed by a mix of Cu and O in different percentage (mostly, cuprite and tenorite), sometimes closed to the eutectic point composition of the Cu-O phase diagram (composition at the eutectic point 14 wt.% O, 86 wt.% Cu; composition of cuprite ≈ 11 wt.% O, ≈ 89 wt.% Cu and of tenorite ≈ 20 wt.% O, ≈ 80 wt.% Cu [37]). Regarding the laser-treated samples, the

inner layer of Test 1 (point C), presenting a composition close to the eutectic point of the Cu-O phase diagram (pie chart C, ≈ 15 wt. % O, ≈ 85 wt. % Cu), is comparable to the composition of the non-treated inner layer. Instead, Test 4 presents only a thinner/densified layer (point D), well bond to the bulk, with a composition close to the typical cuprite composition (pie chart D: ≈ 9 wt. % O, ≈ 91 wt. % Cu).
Comparing these results, it is important to remind that μRaman and EDS spectroscopies are techniques that analyse different volumes. While μRaman analyses the surface (< 1 μm), EDS probes deeper (several micrometres), depending on the used acceleration voltage (> 1 μm at 20 kV). So, μRaman spectra highlighted that the transformation into cuprite occurs only at the surface of the sample, in a depth of less than 1 μm for Tests 1 to 3.

To conclude, the characterisations here exposed strength the compositions previously found by the Authors on the non-treated corroded layers [19]. Moreover, the comparison of the non-treated and laser-treated layers reveals that the performed high irradiance laser-cleaning tests do not substantially modify in composition the artificially-corroded layers. The laser removes the copper chlorides leaving a layer of densified Cu-O compounds, where the possibility of identifying the single crystals is very difficult. Considering the data here exposed and the previous results acquired [19], the differentiated effect of laser irradiation on the two layers is directly related to their different grain size, porosity and diffuse reflectance, and so, the different behaviour. Indeed, the densification of the inner Cu-O layer, with the unaltered presence of the outer copper chloride layer, can be explained with the different reflective behaviour, grain size and porosity of these two layers. The copper chloride layer is composed of bigger grains, which allow a higher penetration of the laser due to a higher transparency to the laser irradiation. Therefore, with low irradiance and fluence values (Test 1), the laser may reach and affect more the inner copper oxides layer and so this explains the densification observed. However, by increasing the irradiance values (Test 4), this high transparency of the outer layer decreases in favour of a higher absorption by scattering along the grain borders, so the copper chloride crystals can be removed and a less affected thin layer of Cu-O compounds remains.
For those reasons, through the EDS analyses, the compounds present in the inner layers were identified as a mix of Cu and O, in different percentage (cuprite/tenorite/eutectic point), probably containing mainly cuprite, as this only phase was detected by Raman

spectroscopy. This can be an indication of the poor crystallinity of the layer, that influences the μRaman results, and the inhomogeneous amount of Cu and O present on the non-treated sample. Nevertheless the formation of a sporadic layer of cuprite due to re-oxidation phenomenon on Test 4 has not been excluded.

3.2. ToF-SIMS characterisations: ^{18}O detection

To assess how the corrosion layer is affected by the laser treatments, ToF-SIMS analyses were performed on the cross-sections of the laser-treated samples. Since the laser treatments were conducted in synthetic air, characterised by the presence of oxygen only in the form of the 18-isotope, any trace of ^{18}O incorporated to the material should be attributed to a laser interaction on the ablated material.

Until now, it was assumed that laser ablation cleaning processes did not alter the composition of either the substrate or the remaining layers. No significant microstructural or elemental composition changes were previously observed. And if the material was affected, it was in the first layers at the atomic or molecular level, given the high selectivity of laser irradiation, but that was not observed for the conditions used in this experiment. The results, illustrated here, suggest that the selected intense laser conditions modify the composition of the artificial corrosion layer. Figure 4 shows particulars of the ToF-SIMS maps obtained from cross-sections analyses of the laser-treated areas (Test 1 to 4). On those maps, a qualitative distribution of a selection of different species present in the corrosion layers after the four Tests can be observed. The maps explain how deep the ^{18}O isotope goes through the cross-section and how its relative distribution is in comparison with other species (^{16}O, Cl^-, Cu^-, C^-). Looking at the maps, the main result to point out is that the ^{18}O is incorporated through the corrosion layer in a homogeneous way. No gradient from the outer surface is observed at this spatial resolution.

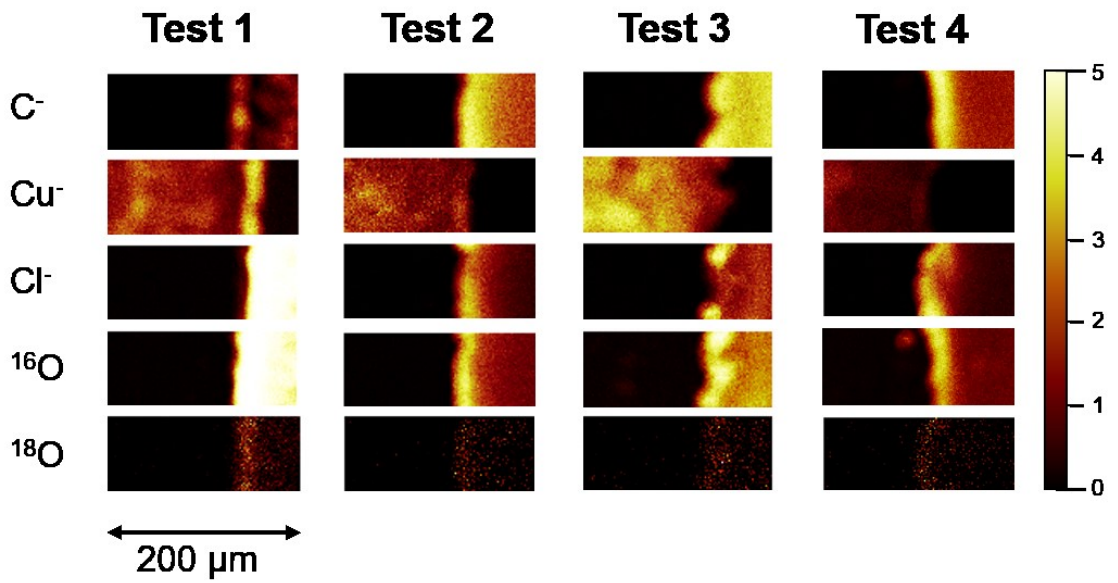

Figure 4: ToF-SIMS maps of the cross-section samples, treated with the four laser Tests conditions chosen to force re-oxidation phenomena during laser treatments (metal on the left and resin on the right).

In addition to the results obtained from the ToF-SIMS maps, Figure 5 plots the oxygen ratio percentage (O_r) and the combined uncertainties (u_c) estimated on the data obtained from the 17 acquisitions, performed on the four laser-cleaning test irradiance conditions, as explained in the methodology part. The horizontal dashed line represents the ^{18}O relative natural abundance, 0.205 at. %, as reported in [28]. The Figure 5 reveals an exponential growth of the ^{18}O % amount as a function of the irradiance values. However, for the lowest irradiance, around 20 MW/cm^2, the measurement uncertainty prevents saying that the laser ablation produces a surface re-oxidation since the increase of ^{18}O % content is small enough to be related to the resolution of the technique.

It should be highlighted that the phenomenon of the re-oxidation can occur either when the corrosion layers are partially removed, with a partial re-oxidation of the remaining layer, or even when they are completely removed, with the formation of, e.g., a thin cuprite layer enriched in ^{18}O.

The results of the ToF-SIMS measurements and the trend of the oxygen ratio allow concluding that surface re-oxidation occurs during the laser treatments carried out at high irradiance values (≈ 74 MW/cm^2). Partial re-oxidation occurs for intermediate laser irradiance (≈ 43 MW/cm^2). On the contrary, negligible re-oxidation may occur for

lower laser irradiance values (lower than ≈ 32 MW/cm^2), taking also into account that below or around irradiance values of ≈ 21 MW/cm^2, the measurement uncertainty prevents to assess the laser effect on possible surface oxidation reactions.

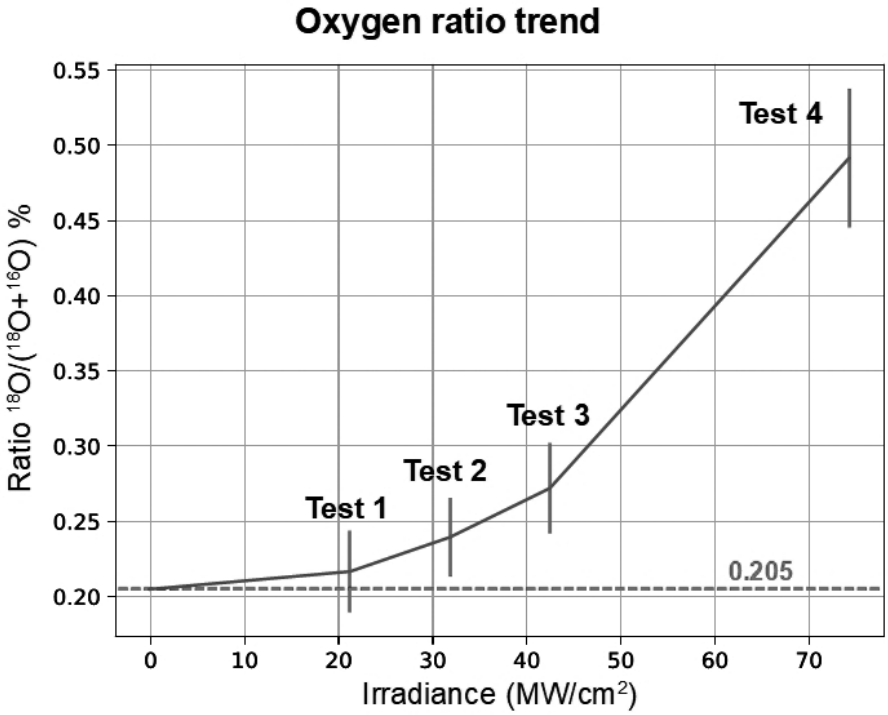

Figure 5: Oxygen ratio trend as a function of the laser irradiance; the dashed line represents the natural abundance of ^{18}O, O_r; the error bars represent the combined uncertainties u_c.

ToF-SIMS analyses demonstrate that oxygen is incorporated several microns in depth into the corrosion layers and even reaching the bulk surface, in the cases where the complete corrosion layer is ablated. In those cases the consequence would be the formation of a layer of cuprite, as observed by μRaman Spectroscopy, of few micrometers thickness. This observation has been made possible only increasing the laser irradiation conditions of the cleaning process above the optimised ones (Test 1).

3.3. Discussion of the proposed ablation mechanism model

As already said, laser irradiation affects more deeply the material than previously thought, suggesting a possible re-oxidation of the corrosion layers (possibly even on the bulk surface).

Figure 6 proposes a schematic representation of how the re-oxidation effect occurs. After laser irradiations, the ablated zones (under the laser beam area) have incorporated

^{18}O, no matter the depth of the layers removed. It is also possible that re-deposited material around the laser-treated area would present an incorporation of ^{18}O that would have occurred during the laser ablation (not the subject of this experiment) [38].

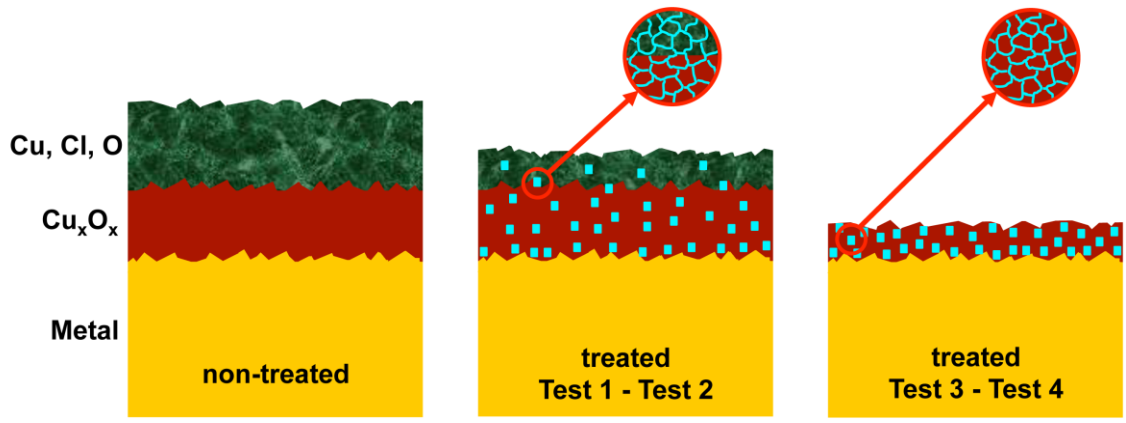

Figure 6: Proposed model of the ablation mechanism for Cu-based alloys: laser-surface material interactions with the oxygen present in the air during laser treatments. The light blue squares depict the ^{18}O incorporation; the *round magnifications* represent the oxygen transport and incorporation through the grain borders (light blue colour).

However, observing structural changes by Raman spectroscopy and only a slight compositional change by EDS, the results suggest that the re-oxidation process returns to its most stable condition similar to the original (according to the kinetics of the phase diagrams) or also that this re-oxidation process occurs only at grain surface, where laser absorption is higher because of the scattering phenomena. A detail of the ^{18}O incorporation into the grain borders is also depicted the round magnifications in Figure 6. This incorporation is directly related with the heating due to thermal ablation [8,27]. Infrared laser irradiation within the nanosecond regime generates an enhancement in the local temperature of the corrosion layer, where photothermal phenomena are the most predominant due to a more efficient electron phonon interaction, above a possible induction of photochemical changes [39]. As previously commented, outer chloride compounds (i.e. clinoatacamite) have higher transmittance than the inner copper oxides (i.e. cuprous oxides), in contact with the copper bulk. This, along with the fact that laser heating advances very fast within the material through the scattering produced in the grain borders, makes the layer suffer a quick heating and posterior cooling. This non-equilibrium heating favours the oxygen transport through the grain borders (light blue in Figure 6 detail), where the oxidation from Cu^+ to its more stable Cu^{2+} state occurs

through the entire layer. That would be an explanation of why the ^{18}O is incorporated in a massive and homogeneous way regardless the quantity. When the heating stops, the shell of Cu^{2+}, already formed around the grains, acts as a diffusion barrier, preventing more oxidation. This shell around the grains is thin enough to avoid the detection of any change in the composition and structure observed by μRaman and FESEM-EDS and μXRD [25,40–42].

To conclude, this result has been acquired when using higher irradiance conditions than the original ones (Test 1). Under normal circumstances it has not been observed in a laser-ablation cleaning process, that is much more sensitive in terms of the appropriate conditions to avoid damaging the remaining layers and the substrate material.

These data allowed proposing a model of the laser-surface material interaction mechanisms during scanning or static laser irradiation. Within the nanosecond regime, re-oxidation processes that take place are mainly related to thermal interactions that favour the intergranular oxygen diffusion inside the corrosion layer.

4. Conclusions

This study shows, for the first time, the combination of a laser-ablation process and an analytical characterisation technique to detect possible transformations during laser irradiation and so allowing the understanding of the laser-material interaction mechanisms involved. A specifically designed novel experimental set-up, with the capability of controlling the mixture of gasses during the process, allowing the incorporation of ^{18}O isotope, made the study of modifications induced by the laser treatments possible. The results obtained show that the oxygen isotope is incorporated to the material surface with the laser treatment. The main results reveal that, in a first characterisation, the laser treatment apparently does not change the elemental or microstructural composition of the corrosion layers, but the amount of incorporated isotope is higher as the irradiance values increase. This is of special relevance in cleaning of corrosion products. During the laser treatment, the layers subjected to be removed suffer a temporal transformation, no matter the depth of the ablation removal. Thermal effects represent the main contribution to the incorporation of the oxygen isotope and the consequent re-oxidation processes happening, with all probability, through the grain borders. This experiment can be considered as a contribution to the systematic study of the ablation processes. The promising presented results are just a

starting point for further studies: the novel approach, introducing the use of the ^{18}O isotope, and the observed incremental trend could lead to further more advanced studies on the laser-surface material processing and modification and on the laser-surface interactions, not only on Cu-based alloys.

Acknowledgements

Dr. R. Lahoz wishes to acknowledge professional support of the CSIC Interdisciplinary Thematic Platform "Open Heritage: Research and Society (PTI-PAIS)".
Dr. E. Di Francia would like to acknowledge the European Federation of Corrosion (EFC) – EUROCORR Young Scientist Grant Selection Committee 2016 that stimulated the initial collaboration that subsequently produced this research.
Dr. V. Rico thanks the FEDER program through AEI-MICINN (PID2019-110430GB-C21) and Junta de Andalucía (PAIDI-2020 through project P18-RT-3480) for financial support

References

1. Hitz, C. B., Ewing, J. & Hecht, J. *Introduction to Laser Technology: Fourth Edition*. *Introduction to Laser Technology: Fourth Edition* (2012). doi:10.1002/9781118219492.
2. Madhukar, Y. K., Mullick, S., Shukla, D. K., Kumar, S. & Nath, A. K. Effect of laser operating mode in paint removal with a fiber laser. *Appl. Surf. Sci.* (2013) doi:10.1016/j.apsusc.2012.10.193.
3. Ahn, D., Jang, D., Park, T. & Kim, D. Laser removal of lubricating oils from metal surfaces. *Surf. Coatings Technol.* (2012) doi:10.1016/j.surfcoat.2012.03.028.
4. Deschênes, J. M. & Fraser, A. Empirical Study of Laser Cleaning of Rust, Paint, and Mill Scale from Steel Surface. in *Minerals, Metals and Materials Series* (2020). doi:10.1007/978-3-030-36556-1_17.
5. Guan, Y. C. *et al.* Laser surface cleaning of carbonaceous deposits on diesel engine piston. *Appl. Surf. Sci.* (2013) doi:10.1016/j.apsusc.2013.01.075.
6. Dutta Majumdar, J. & Manna, I. Laser material processing. *Int. Mater. Rev.* (2011) doi:10.1179/1743280411Y.0000000003.
7. Zhang, S. L. *et al.* Mechanisms of laser cleaning induced oxidation and corrosion property changes in AA5083 aluminum alloy. *J. Laser Appl.* (2019)

doi:10.2351/1.5046470.

8. Bäuerle, D. W. *Laser processing and chemistry*. (Springer, 2011).
9. Rhodes, E. W. T. *et al. Laser Ablation and its applications*. *Springer Series in Optical Sciences* (2007). doi:10.1007/978-0-387-30453-3.
10. Sidot, E., Souissi, N., Bousselmi, L., Triki, E. & Robbiola, L. Study of the corrosion behaviour of Cu-10Sn bronze in aerated Na2SO4 aqueous solution. *Corros. Sci.* (2006) doi:10.1016/j.corsci.2005.08.020.
11. Ingo, G. M. *et al.* Large scale investigation of chemical composition, structure and corrosion mechanism of bronze archeological artefacts from Mediterranean basin. *Appl. Phys. A Mater. Sci. Process.* (2006) doi:10.1007/s00339-006-3550-z.
12. FitzGerald, K. P., Nairn, J., Skennerton, G. & Atrens, A. Atmospheric corrosion of copper and the colour, structure and composition of natural patinas on copper. *Corros. Sci.* (2006) doi:10.1016/j.corsci.2005.09.011.
13. Ospitali, F. *et al.* The characterization of Sn-based corrosion products in ancient bronzes: A Raman approach. in *Journal of Raman Spectroscopy* (2012). doi:10.1002/jrs.4037.
14. Fotakis, C., Anglos, D., Zafiropulos, V., Georgiou, S. & Tornari, V. *Lasers in the Preservation of Cultural Heritage: Principles and Applications*. *Series in Optics and Optoelectronics* (2007).
15. Siano, S., Salimbeni, R., Pini, R., Giusti, A. & Matteini, M. Laser cleaning methodology for the preservation of the Porta del Paradiso by Lorenzo Ghiberti. *J. Cult. Herit.* (2003) doi:10.1016/s1296-2074(02)01138-x.
16. Drakaki, E. *et al.* Laser cleaning on Roman coins. in *Applied Physics A: Materials Science and Processing* (2004). doi:10.1007/s00339-004-2657-3.
17. Siano, S. *et al.* Laser cleaning in conservation of stone, metal, and painted artifacts: State of the art and new insights on the use of the Nd:YAG lasers. *Appl. Phys. A Mater. Sci. Process.* (2012) doi:10.1007/s00339-011-6690-8.
18. Siano, S. & Salimbeni, R. Advances in laser cleaning of artwork and objects of historical interest: The optimized pulse duration approach. *Acc. Chem. Res.* (2010) doi:10.1021/ar900190f.
19. Di Francia, E., Lahoz, R., Neff, D., Angelini, E. & Grassini, S. Laser cleaning of Cu-based artefacts: Laser/corrosion products interaction. *Acta IMEKO* **7**, (2018).
20. Yonezawa, Y., Minamikawa, T., Morimoto, A. & Shimizu, T. Removal of surface oxides on copper by pulsed laser irradiation. *Japanese J. Appl. Physics, Part 1*

Regul. Pap. Short Notes Rev. Pap. (1998) doi:10.1143/jjap.37.4505.

21. FOTAKIS, C. LASERS FOR ART'S SAKE! *Opt. Photonics News* (1995) doi:10.1364/opn.6.5.000030.
22. Matteini, M., Lalli, C., Tosini, I., Giusti, A. & Siano, S. Laser and chemical cleaning tests for the conservation of the Porta del Paradiso by Lorenzo Ghiberti. *J. Cult. Herit.* (2003) doi:10.1016/s1296-2074(02)01190-1.
23. Liu, B. W., Mi, G. Y. & Wang, C. M. Reoxidation process and corrosion behavior of TA15 alloy by laser ablation. *Rare Met.* (2020) doi:10.1007/s12598-020-01553-8.
24. Seo, C., Ahn, D. & Kim, D. Removal of oxides from copper surface using femtosecond and nanosecond pulsed lasers. *Appl. Surf. Sci.* (2015) doi:10.1016/j.apsusc.2015.05.011.
25. Dajnowski, B. A. *et al.* Creating Laser Patinas on Copper Alloys : Origins of Colors and their Implications on Copper Alloys. in *Metal 2016 Proceedings of the Interim Meeting of the ICOM-CC Metals Working Group September 26-30, 2016 New Delhi, India* (2017).
26. Kaczkowski, R. A., Dajnowski, B. A. & Vicenzi, E. P. From Earth to Outer Space: Laser cleaning semiprecious quartz and a novel application for meteoritic metal. in (2017). doi:10.12775/3875-4.03.
27. Rubahn, H. *Laser Applications in Surface Science and Technology*. (Wiley, 1999).
28. Lide, D. R. CRC Handbook of Chemistry and Physics, Internet Version 2005. *CRC Press. Taylor Fr. Boca Rat. FL* (2005) doi:10.1016/0165-9936(91)85111-4.
29. Casaletto, M. P., De Caro, T., Ingo, G. M. & Riccucci, C. Production of reference 'ancient' Cu-based alloys and their accelerated degradation methods. *Appl. Phys. A Mater. Sci. Process.* (2006) doi:10.1007/s00339-006-3545-9.
30. Lafuente, B., Downs, R. T., Yang, H. & Stone, N. The power of databases: The RRUFF project. in *Highlights in Mineralogical Crystallography* (2016). doi:10.1515/9783110417104-003.
31. Bouchard-Abouchacra, M. Evaluation des Capacités de la Microscopie Raman dans la Caractérisation Minéralogique et Physico- chimique de Matériaux Archéologiques - Métaux, Vitraux & Pigments. (École doctorale Sciences de la nature et de l'Homme - Évolution et écologie (Paris), 2001).
32. Piccardo, P., Mille, B. & Robbiola, L. Tin and copper oxides in corroded archaeological bronzes. in *Corrosion of Metallic Heritage Artefacts: Investigation,*

Conservation and Prediction of Long Term Behaviour (2007). doi:10.1533/9781845693015.239.

33. Soffritti, C., Fabbri, E., Merlin, M., Garagnani, G. L. & Monticelli, C. On the degradation factors of an archaeological bronze bowl belonging to a private collection. *Appl. Surf. Sci.* (2014) doi:10.1016/j.apsusc.2014.06.067.
34. Frost, R. L. Raman spectroscopy of selected copper minerals of significance in corrosion. *Spectrochim. Acta - Part A Mol. Biomol. Spectrosc.* (2003) doi:10.1016/S1386-1425(02)00315-3.
35. Bertolotti, G. *et al.* Micro-Raman study of copper hydroxychlorides and other corrosion products of bronze samples mimicking archaeological coins. *Anal. Bioanal. Chem.* (2012) doi:10.1007/s00216-011-5268-9.
36. Mineralogy Database. *Choice Rev. Online* (2007) doi:10.5860/choice.45-0296.
37. Massalski, T. B., Okamoto, H., Subramanian, P. R. & Kacprzak, L. *Binary Alloy Phase Diagrams: Ni-S. American Society for Metals1128* (1990).
38. Lahoz, R., Espinós, J. P., de la Fuente, G. F. & González-Elipe, A. R. 'in situ' XPS studies of laser induced surface cleaning and nitridation of Ti. *Surf. Coatings Technol.* (2008) doi:10.1016/j.surfcoat.2007.06.061.
39. Lahoz, R., Espinós, J. P., Yubero, F., González-Elipe, A. R. & De La Fuente, G. F. In situ XPS studies of laser-induced surface nitridation and oxidation of tantalum. *J. Mater. Res.* (2015) doi:10.1557/jmr.2015.190.
40. Froidevaux, M., Piatt, P., Cooper, M. & Watkins, K. Laser interactions with copper, copper alloys and their corrosion products used in outdoor sculpture in the United Kingdom. in *Lasers in the Conservation of Artworks - Proceedings of the International Conference LACONA 7* (2008). doi:10.1201/9780203882085.pt6.
41. Murali, D. S. & Aryasomayajula, S. Thermal conversion of Cu4O3 into CuO and Cu2O and the electrical properties of magnetron sputtered Cu4O3 thin films. *Appl. Phys. A Mater. Sci. Process.* (2018) doi:10.1007/s00339-018-1666-6.
42. Raship, N. A., Sahdan, M. Z., Adriyanto, F., Nurfazliana, M. F. & Bakri, A. S. Effect of annealing temperature on the properties of copper oxide films prepared by dip coating technique. in *AIP Conference Proceedings* (2017). doi:10.1063/1.4968374.

LIST OF FIGURES

TABLES